Available online at www.sciencedirect.com
SCIENCE DIRECT®
Journal of Magnetic Resonance 177 (2005) 1–8
JMR Journal of Magnetic Resonance
www.elsevier.com/locate/jmr

Ultra-wide bore 900 MHz high-resolution NMR at the National High Magnetic Field Laboratory

R. Fu [a], W.W. Brey [a], K. Shetty [a], P. Gor'kov [a], S. Saha [a], J.R. Long [b], S.C. Grant [b], E.Y. Chekmenev [a], J. Hu [a], Z. Gan [a], M. Sharma [c], F. Zhang [a], T.M. Logan [c], R. Brüschweller [a], A. Edison [b], A. Blue [a], I.R. Dixon [a], W.D. Markiewicz [a], T.A. Cross [a,c,*]

[a] *National High Magnetic Field Laboratory, 1800 East Paul Dirac Drive, Tallahassee, FL 32310, USA*
[b] *McKnight Brain Institute, University of Florida, Gainesville, FL 32610, USA*
[c] *Department of Chemistry and Biochemistry, Florida State University, Tallahassee, FL 32306, USA*

Received 10 June 2005; revised 7 July 2005
Available online 25 August 2005

Abstract

Access to an ultra-wide bore (105 mm) 21.1 T magnet makes possible numerous advances in NMR spectroscopy and MR imaging, as well as novel applications. This magnet was developed, designed, manufactured and tested at the National High Magnetic Field Laboratory and on July 21, 2004 it was energized to 21.1 T. Commercial and unique homebuilt probes, along with a standard commercial NMR console have been installed and tested with many science applications to develop this spectrometer as a user facility. Solution NMR of membrane proteins with enhanced resolution, new pulse sequences for solid state NMR taking advantage of narrowed proton linewidths, and enhanced spatial resolution and contrast leading to improved animal imaging have been documented. In addition, it is demonstrated that spectroscopy of single site ^{17}O labeled macromolecules in a hydrated lipid bilayer environment can be recorded in a remarkably short period of time. ^{17}O spectra of aligned samples show the potential for using this data for orientational restraints and for characterizing unique details of cation binding properties to ion channels. The success of this NHMFL magnet illustrates the potential for using a similar magnet design as an outsert for high temperature superconducting insert coils to achieve an NMR magnet with a field >25 T.

Keywords: 900 MHz superconducting magnet; Solution NMR; Solid State NMR; MR microscopy; Transmission line NMR probe

1. Introduction

The struggle to achieve higher magnetic field strengths for NMR has been primarily motivated by a fundamental need for resolution and sensitivity, but there are many other advantages associated with high magnetic fields. In general, these advantages are not applicable to all experiments or to all sample applications. However, these advantages often have a multiplicative effect, for instance an improvement in resonance linewidth, from a change in relaxation rates or improved sample orientation, not only improves spectral resolution, but also improves sensitivity. Consequently, an incremental improvement in field strength can often lead to dramatic advantages for the spectroscopy or imaging of specific molecular systems. Here, we illustrate a few high field advantages through spectra obtained on the 105 mm room temperature bore 21.1 T magnet at the National High Magnetic Field Laboratory (NHMFL).

In July, 2004 this project funded by the National Science Foundation was brought to fruition when this superconducting NMR magnet was energized to full field. Here, we report on initial scientific findings from this unique magnet.

* Corresponding author. Fax: +1 850 644 1366.
E-mail address: cross@magnet.fsu.edu (T.A. Cross).

1090-7807/$ - see front matter © 2005 Elsevier Inc. All rights reserved.
doi:10.1016/j.jmr.2005.07.013

2. Ultra-wide bore 900 MHz NMR spectrometer

2.1. Superconducting magnet

The ultra-wide bore 900 MHz superconducting NMR magnet was developed, designed, manufactured, and tested by a team of engineers at the NHMFL and an industrial partner, Intermagnetics General [1–7]. Bringing the world's largest NMR magnet to operation marks a significant achievement in magnet technology and this milestone was achieved without incurring any training quenches in the final cryostat. This cryostat, shown in Fig. 1, stands 4.9 m (16 feet) tall, weighs over 13,600 kg (30,000 lb), and has a stored energy of 38 MJ.

The magnet is a concentric assembly of 10 superconducting coils connected in series. Each of the coils is wound with a monolithic superconductor, composed of either niobium–tin (Nb_3Sn) or niobium–titanium (NbTi) filaments in a copper matrix. The coils are reinforced with stainless steel bands and are vacuum impregnated with cryogenically tough epoxy for structural support. The magnet resides within a vessel of the cryostat containing 2400 L liquid helium at atmospheric pressure. This "magnet vessel" is conductively cooled to a temperature of 1.7 K by use of a closed loop heat exchanger. The pressure of the saturated helium in the heat exchanger is reduced to achieve the superfluid conditions. The level of helium in the heat exchanger is controlled by a Joule–Thompson (JT) valve that draws liquid in from the 1100 L Helium-I reservoir. This liquid, prior to going through the JT-valve, is precooled to near the lambda point, T_λ, by the vapor that is being pumped off. The cryostat also contains a number of thermal shields and multi-layer insulation to suppress the radiative heat loads.

Fig. 1. Ultra wide bore 900 MHz NMR magnet system at the National High Magnetic Field Laboratory.

The 900 MHz magnet was originally conceived as a prototype for the outer coils of a standard bore 1.1 GHz (25 T) NMR magnet in which the field exceeds the operational limits of conventional low temperature superconductors (LTS) [8]. A 25 T magnet would require the innermost coils to be constructed of high temperature superconductors (HTS). The HTS coil would produce 5 T with the remaining LTS coils producing 20 T. The 900 MHz magnet is of the same scale as a 1.1 GHz magnet, but its innermost coil is constructed of LTS, which adds an additional 1.1 T for a total central field of 21.1 T and a large cold bore inner diameter of 140 mm.

After reaching 21.1 T, an initial adjustment of the superconducting shims was performed to achieve a magnet homogeneity of approximately ±2 ppm over a 4-cm sphere [9]. An 18-channel room temperature (RT) shim set, with an inner diameter of 89 mm, developed by Resonance Research Inc. (RRI), was installed to further improve the uniformity to ±0.1 ppm in a cylinder 17 mm in diameter and 35 mm in height and to ±5 ppb over a 1 cm DSV at the center of the field, which is sufficient for imaging and solid-state NMR. A second standard bore RT shim set provided by Bruker Biospin is being used for high resolution solution NMR.

Measured within a few days of achieving the field, the decay rate was 523 Hz/h. Over the subsequent 9 months, the decay rate has decreased slightly to 498 Hz/h, a change of 2 Hz/month. Because the stability required for NMR applications is typically 5–10 Hz/h, it was necessary to find some ways to compensate for the drift. The drift was discovered during preliminary tests of the magnet before it was inserted into the final cryostat. Measurements of voltages across the various coil sections indicated that the decay is most likely due to a defect near one of the persistent joints. Several methods for compensating drift in NMR magnets have been proposed [10,11], but were not practical to implement. A new method of current injection was proposed and tested [12] that required minimal modification to the magnet to inject current through low loss leads into one of the main superconducting coils. As constructed, this system is capable of correcting for field drift over a continuous period of >1000 h. Short term tests at 16.9 T indicated that this compensation system would operate as designed. However, we have chosen not to operate this system routinely because it increases, however slightly,

some risk for the magnet and cryostat, and a satisfactory alternative is available. Instead, we have simply applied a current ramp to the Z_0 coil of the RRI shim set. This allows drift compensation for about 5.3 days, as shown in Fig. 2, before it is necessary to reset the current source and the spectrometer frequency. To date, there has been no evident problem with either bore heating or B_0 homogeneity associated with the Z_0 coil ramp, and the maximum ramp period has not limited the duration of NMR experiments. If any of these issues become significant, the current injection system can be employed.

It is worth noting that the magnet needs to be re-energized to 900 MHz when it drifts beyond the frequency range of hardware in the console (such as the ^{1}H preamplifier) or the ^{1}H tuning range of the probes. Based on the current drift rate, the magnet will be re-energized once a year with the first boost in field planned for August 2005.

2.2. NMR spectroscopy

All NMR experiments were performed on a 4-channel Bruker Avance 900 MHz console with solution, solid state, and micro-imaging NMR capabilities. The NMR console is equipped with ^{1}H/^{19}F solid state amplifiers (100 W output for solution and 800 W for solid state NMR), and one 1000 W and two 500 W amplifiers for broadband irradiation. The console also has 60-A triple axis gradient amplifiers for imaging and diffusion NMR experiments.

For solution NMR experiments, a Bruker 5-mm inverse triple resonance ^{1}H{^{13}C, ^{15}N} probe with a ^{2}H lock was used. With the standard bore RT shim set, a ^{1}H sensitivity of 1946:1 was achieved for ethylbenzene in $CDCl_3$. The ^{1}H lineshape and resolution for the standard test sample of $CHCl_3$ in acetone were characterized by 6.6/7.9 and 0.65 Hz, respectively. This probe includes actively shielded X, Y, and Z gradient coils with variable temperature control.

A Bruker Doddrell micro-imaging probe system was used in imaging measurements. The system includes linear birdcage coils with inner diameters of 5, 10, and 30 mm and a 3-mm diameter solenoid.

For solid state magic angle spinning (MAS) NMR experiments, a 3.2-mm Bruker HCN triple resonance MAS NMR probe was used. The observed ^{13}C linewidth at half height for the NMR resonances of natural abundance adamantane was 4.3 Hz with good lineshape, indicating that the RRI's 18-channel RT shims provide sufficient field homogeneity for high resolution solid state NMR experiments. In addition, static solid-state ^{17}O and ^{15}N NMR experiments were carried out using a home-made ^{1}H–X transmission line NMR probe with interchangeable sample coils described in detail below. Temperature of the sample chamber was controlled to within ± 0.1 K using a Bruker BVT-3000 temperature control unit.

3. Research on the 900 MHz magnet

3.1. Solution NMR spectroscopy

Solution NMR studies of integral membrane proteins are intrinsically challenging due to the need for a lipophilic phase for solubilizing these proteins into an aqueous solution. Detergent micelles containing integral membrane proteins typically result in particles larger than 50 kDa. Such preparations often give rise to broad resonances due to slow correlation times for the overall

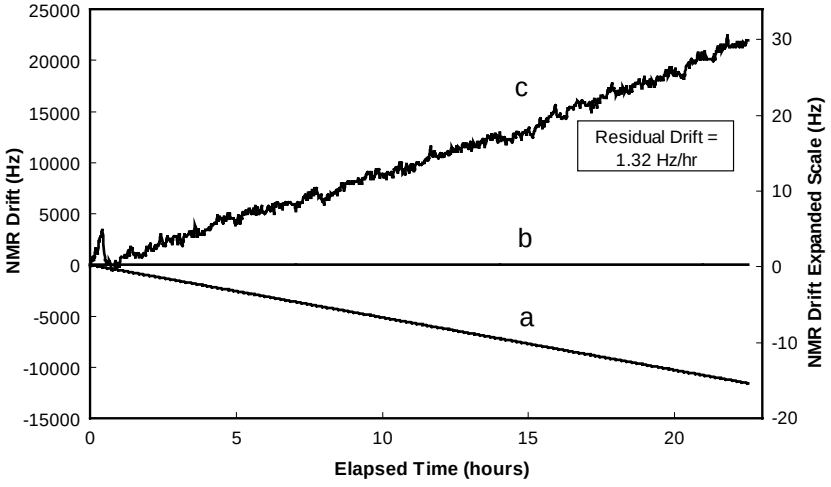

Fig. 2. Drift compensation at 900 MHz for a period of 24 h, achieved by a constant field ramp in the Z_0 coil of the RT shim tube. The uncompensated drift (a) was previously measured to be 512 Hz/h. The residual drift (b) after compensation was reduced to 1.32 Hz/h. (The expanded scale is shown in (c).) Even higher quality compensation could be achieved by providing an accurate value of the drift rate parameter to the control system. Correction through the Z_0 coil in the RRI shim tube provides drift compensation for a period of about 5.3 days.

tumbling rate. While this appears to be the typical situation there are occasions when the linewidths appear to be narrower than would be predicted by the global correlation time of the complex (personal communication with Prof. Lukas K. Tamm). In addition, detergent solubilized membrane proteins often display heterogeneous linewidths, presumably due to local dynamics. Such local dynamics may also interfere with TROSY's ability to narrow the resonance lines [13].

Here, the M2 protein of influenza A virus, which has 97 residues including a 19 residue transmembrane helix, forms a homo-tetrameric proton channel that acidifies the viral interior during endocytosis and thereby facilitates viral infection. This homo-tetrameric assembly is activated at low pH and inhibited by influenza drugs, amantidine and rimantidine. M2 protein is a potential paradigm system for functional, dynamic and structural studies of viral ion channels and other proton channels. The three-dimensional structure of the transmembrane domain has been solved using solid state NMR (PDB #1NYJ) [14], but the structure and functional analysis of the full-length M2 protein still remains elusive. Fig. 3 shows the ^{15}N–^{1}H TROSY spectrum of 1 mM M2 protein in detergent micelles at pH 4 obtained at 900 MHz. This sample is a cysteine linked dimer and, based on cross-linking studies, appears to be a tetramer. With higher resolution and better signal-to-noise achieved on the 900 MHz spectrometer, more than 95% of the expected peaks in the M2 protein have been identified. Such results represent a major step toward achieving resonance assignments, essential for structural and functional studies of the protein.

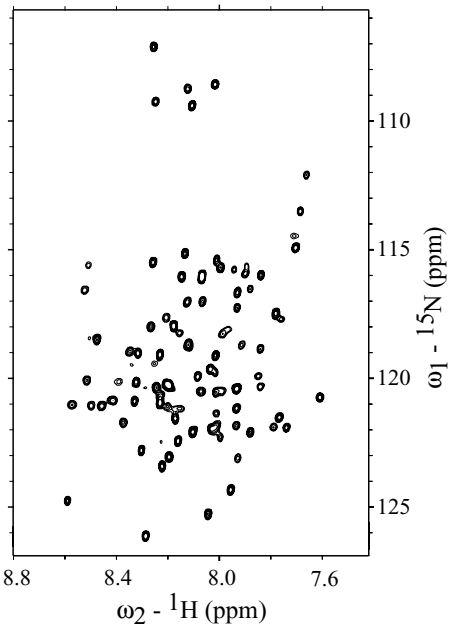

Fig. 3. ^{15}N–^{1}H TROSY spectra of 1 mM M2 protein in DPC micelles at pH 4 obtained at 900 MHz. The protein is a covalent dimer of 97 amino acid residues and appears to be a tetramer under these experimental conditions (see text). The spectrum was obtained with 32 scans and 256 increments in the indirect dimension with a recycle delay of 1 s.

Although solution NMR rarely requires a wide bore magnet, high quality TROSY spectra obtained at 900 MHz clearly indicate that both the homogeneity and stability of this ultra-wide bore 900 MHz magnet are sufficient enough for high resolution solution NMR spectroscopy. Many of the solution multi-dimensional NMR experiments for protein structural characterization have been demonstrated using a standard ubiquitin sample.

3.2. Solid-state NMR spectroscopy

Biological ^{17}O NMR is intrinsically challenging due to low sensitivity and resolution resulting from the low gyromagnetic ratio, low natural abundance (~0.038%), and large quadrupolar interactions [15]. Since many carbonyl oxygens in proteins actively participate in a variety of biological functions, ^{17}O NMR spectroscopy would permit direct studies of these sites.

Fig. 4 shows the ^{17}O NMR spectra of aligned ^{17}O-[D-Leu$_{10}$]-gramicidin A (gA) with and without the presence

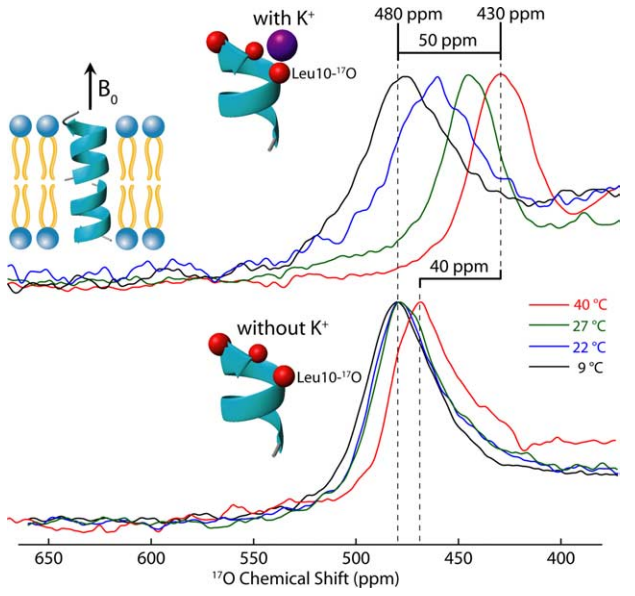

Fig. 4. ^{17}O NMR spectra of ^{17}O-[D-Leu$_{10}$]-gA uniformly aligned in DMPC bilayers in the absence and the presence of KCl (2.4 M) with a peptide:lipid ratio of 1:16. The ^{17}O-[D-Leu$_{10}$]-gA was prepared by solid-phase peptide synthesis from corresponding Fmoc derivatives. Fmoc-^{17}O-D-Leu was synthesized from ^{17}O-D-Leu, enriched at 57% by acid-catalyzed exchange [32]. Each sample containing less than 3 μmol ^{17}O labeled [D-Leu$_{10}$]-gA was oriented between 30 μm thick glass slides following the literature procedure [19]. All spectra were recorded using the standard spin echo pulse sequence and phase-corrected over the entire spectral width of 500 ppm. No ^{1}H decoupling was employed in the experiments and the ^{17}O B_1 field used was 42 kHz with a recycle delay of 8 ms. About 2–4 h of signal averaging time was used to collect each NMR spectrum. The ^{17}O chemical shift of H_2O was referenced as 0 ppm.

of K^+. GA is a 15-residue polypeptide with an alternating sequence of D- and L-amino acids forming a right-handed β-helical homodimeric channel structure with a 4.5 Å pore in hydrated DMPC lipid bilayers [16–18]. It was previously shown through ^{15}N anisotropic chemical shifts [19] that the carbonyl oxygen of D-Leu_{10} is one of three sites involved in cation binding. It is known that the most deshielded chemical shift (CS) tensor component, δ_{11}, is oriented close to the C=O bond and is extremely sensitive to ion binding. For samples with the bilayer normal uniformly aligned parallel to the magnetic field, the Leu_{10} δ_{11} tensor element is almost parallel to B_0 [19] and consequently the observed anisotropic CS in Fig. 4 are close to δ_{11} (480 ppm). While linewidths appear quite broad, which results in large part from fast quadrupolar relaxation, they are, in fact, relatively narrow compared to the CS anisotropy and despite the broad lines sensitivity is very high. In the absence of the K^+ cations, the position of the anisotropic ^{17}O chemical shift resonance does not change at temperatures below 27 °C (cf. Fig. 4) but shifts by about 10 ppm above the lipid's phase transition temperature as rapid global motion of gA is induced about the bilayer normal.

In the presence of 2.4 M KCl, at least 80% of the gA channels are doubly occupied, i.e., one ion per monomer [19,20]. Above the phase transition temperature, the ^{17}O NMR resonance shifts by as much as 40 ppm upon the addition of K^+. It has been hypothesized [21] that ions bound to gA are delocalized over carbonyls 10, 12, and 14 exposed at the channel entrance and exit. Apparently, the time-averaged K^+ position is more distant from the Leu_{10} site as the temperature is lowered below the phase transition and at 9 °C there is no longer any evidence of an interaction between K^+ and the carbonyl oxygen. Possibly, the potential energy profile for ion binding is influenced by the dramatic increase in the bilayer thickness below the lipid phase transition. Importantly, the principles of ion binding and conductance across the membrane learned here are similar to those in ion selective channels such as the K^+ channel, KcsA. Thus, this ^{17}O NMR approach for characterizing ion binding carbonyl sites has considerable potential.

One of the major problems in protein structural characterization using PISEMA data is the degenerate solutions associated with the orientational restraints. Generally, a peptide plane has four possible orientations with respect to B_0 that fulfill the same ^{15}N chemical shift and ^{15}N–^1H dipolar coupling. With better ^1H resolution at 900 MHz, it will be possible to introduce ^1H anisotropic chemical shift restraints into the structural determination to eliminate some of the degeneracies. Fig. 5 shows the anisotropic ^1H–^{15}N chemical shift correlation spectrum of a static ^{15}N-acetyl-valine crystal at 900 MHz recorded with and without ^{15}N decoupling during ^1H chemical shift evolution. Two ^{15}N resonances

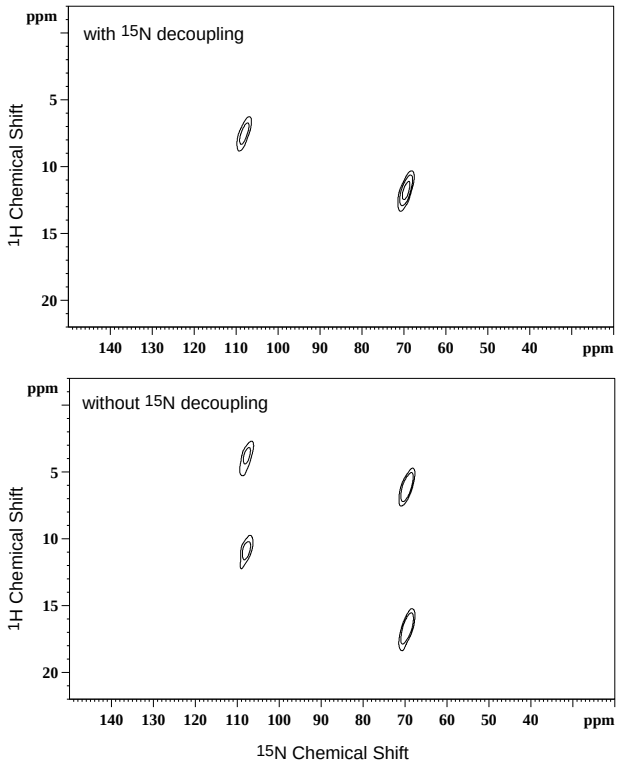

Fig. 5. ^{15}N–^1H correlation spectra of a NAV crystal at 900 MHz with (top) and without (bottom) ^{15}N decoupling during the ^1H chemical shift evolution. The magic sandwich high order truncation (MSHOT) homonuclear decoupling sequence [23] was used in the t_1 dimension. A short cross-polarization contact time of 120 μs was used to ensure that the ^{15}N magnetization was transferred from its closest ^1H. The ^1H B_1 fields were 92 and 50 kHz during the MSHOT decoupling and cross-polarization, respectively, while the ^{15}N B_1 field of 50 kHz was used for cross-polarization and ^{15}N decoupling in the t_1 dimension. The quadruture detection in the t_1 dimension was achieved using the states phase cycling. In the spectra, the scaling factor has been taken into account in the ^1H chemical shift dimension. The ^1H chemical shift was referenced to the water signal in NH_4NO_3 solution at 4.7 ppm.

were observed at this arbitrary orientation due to the existence of two inequivalent molecules per unit cell in the crystal [22]. After considering the scaling factor in the ^1H chemical shift dimension, resulting from ^1H homonuclear dipolar decoupling [23], the ^1H linewidth was 1.2 ppm, while it was 2.1 ppm from the same crystal sample at 300 MHz. Without ^{15}N decoupling, the corresponding ^1H–^{15}N dipolar couplings split each of the resonances into doublets. Therefore, such experiments allow us to obtain the ^1H–^{15}N dipolar couplings, as in PISEMA experiments [24], and to acquire the additional anisotropic ^1H chemical shift restraints, without a need to perform time-consuming three-dimensional experiments [25,26].

3.3. MR microscopy

At high magnetic field strengths, a large number of anatomical structures can be defined accurately in magnetic resonance microscopy (MRM) [27–29]. The

growing potential for applications of MRM technology in the arenas of morphology, gene expression, and nanotechnology has increased the need for comprehensive microimaging of rodent neuroanatomy with accurate segmentation of structures as well as quantitative analysis of MR parameters. It is widely recognized that numerous MR contrast mechanisms (T_1, T_2, and T_2^*) are dependent upon magnetic field strength, offering opportunities for enhanced and emergent contrast mechanisms at high fields. Additionally, high fields provide increased signal, which can be utilized to increase spatial resolution or decrease acquisition times. Finally, the bore size of the 900-MHz UWB system provides a unique opportunity for MRM to be extended to sample sizes beyond the capability of existing microimaging systems. These samples potentially include large in vivo rodents (adult rats, guinea pigs, etc.) as well as sizeable ex vivo specimens.

As shown in Fig. 6, the gradient-recall echo images of an excised, perfusion-fixed C57BL/6J mouse brain acquired with a 10-mm linear birdcage coil at 900 MHz illustrate the great potential of MR microscopy at high fields. The axial image of Fig. 6 (top) is a slice from a three-dimensional data set with a resolution of $18 \times 18 \times 35$ μm in 29 h. The spatial resolution permits clear visualization of layering in both the cortex and cerebellum as well as white matter fibers in the corpus callosum, cerebellum and olfactory bulbs. The four coronal images at the bottom of Fig. 6 were acquired in 10 min using a multi-slice sequence with a resolution of $40 \times 40 \times 250$ μm. Clockwise from the upper left, the images display increasing T_2^* weighting with echo times increasing from 4.5 to 24.5 ms. To underscore the homogeneity of this system, the increase in tissue contrast with increasing T_2^* weighting is not significantly diminished by either a significant loss in signal-to-noise ratio or a drastic increase in undesirable susceptibility artifacts. Again, these coronal images display distinct structural features, particularly in the hippocampus where individual cellular layers can be identified because of the superior T_2^* contrast.

Fig. 6. Gradient-recall echo images of an excised, perfusion-fixed C57BL/6J mouse brain in a 10-mm linear birdcage recorded at 21.1 T. A true 3D gradient-recall echo dataset was acquired at a resolution of $18 \times 18 \times 35$ μm in 29 h using the following imaging parameters: matrix = $1024 \times 512 \times 256$; TE/TR = 12.5/100 ms; averages = 8; FOV = $1.9 \times 0.92 \times 0.8$ cm; bandwidth = 100 kHz; 50° tip angle = 25-μs hard pulse. A series of 2D multi-slice gradient-recall echo images ($40 \times 40 \times 250$-μm resolution) were acquired to sample T_2^* using the following parameters: matrix = 230×200; TE = 4.5–24.5 ms; TR = 1.5 s; averages = 2; FOV = 9.2×8.0 mm; slice thickness = 250 μm; number of slices = 17; 90° pulse = 2-ms three-lobe sinc pulse; and imaging time per dataset = 10 min.

3.4. ^1H–X broadband transmission line probe at high fields

The well known transmission line probe [30,31] consists of a single sample coil, a low RF loss transmission line, and a matching network mounted outside the magnet. This probe has an efficient low frequency detection channel. However, in a physically long, high field magnet, this approach leads to unacceptable loss in the high frequency ^{1}H channel. For example, in the 900 UWB magnet, the distance from the field center to the magnet flange is >1.5 m and spans almost five wavelengths. An additional disadvantage of the conventional design for high frequency ^{1}H operation is the B_1 inhomogeneity associated with its unbalanced RF coil, and its undesirable effect on cross-polarization efficiency. To make it more useful in the 900 UWB, our homebuilt transmission line probe design has been modified as follows: high frequency loss has been reduced by locating tuning and matching capacitors within the bore of the magnet—1/

4λ to $1/2\lambda$ below the coil. Correction of B_1 homogeneity was made by having a portion of probe's RF shield serve as a sleeve balun to electrically balance the sample coil at the ^{1}H frequency. With these two modifications, the original transmission line design can be efficiently used in long bore, high field magnets such as the NHMFL 900 UWB.

Fig. 7 shows a schematic diagram of the probe. Because of their low RF loss, 75 Ω air coaxial cables were used throughout. The lengths of three coaxial cables from point 'b' to points 'a,' 'c,' and 'd' are critical for proper functioning of the probe: to transfer maximum power to the sample coil and to create the maximum B_1 field. [31] The optimal lengths of the cables depend on the impedance of the RF coil and the operating frequency. The probe shield, which is a grounded $1/4\lambda$ away from point 'a,' acts as ''sleeve balun'' and electrically balances the sample coil at the ^{1}H frequency. The coaxial cable from 'a' to 'b' is used to create a voltage node at 'b,' while the cable length between 'b' and 'c' aids in ^{1}H tuning. For proper isolation between two channels, a cable is added from point 'b' to 'd.' The latter cable is nearly a $1/4\lambda$ long, thus producing high impedance at point 'b' and reducing the transfer of power at the ^{1}H frequency to the X observe port. At the lower X frequency, the low ac resistance of the large diameter (0.375″) center conductor in the transmission line between points 'd' and 'a' ensures that most of the power in the X observe port dissipates in the sample coil and not in the matching network. Capacitor C5 serves to balance the sample coil at the observe frequency, reducing the voltage across the circuit and allowing for higher power experiments.

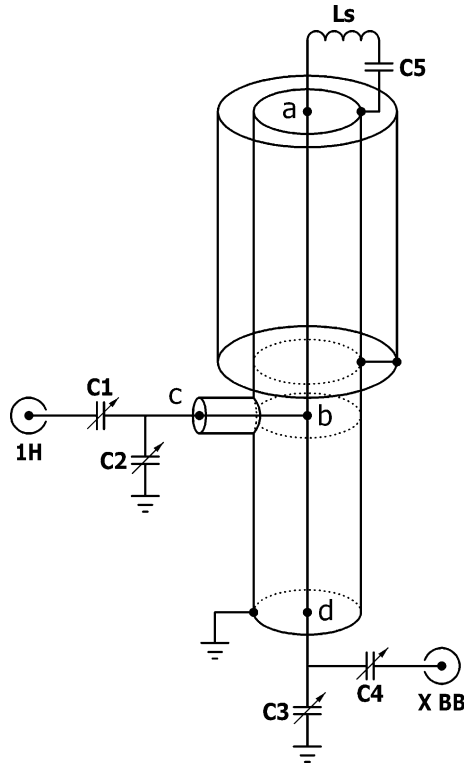

Fig. 7. Diagram of 900 MHz compact transmission line probe.

This modified, double-tuned compact transmission line probe for a high field magnet provides an efficient low frequency observe channel while preserving the performance and homogeneity of the ^{1}H channel. For example, at the ^{1}H frequency (900 MHz), 170 kHz B_1 fields were achieved with 250 W of input power using a 4.1-mm ID solenoid sample coil (5.5 mm long, 4.5-turns), with the RF homogeneity $A_{810^\circ}/A_{90^\circ}$ ~80% over the 5-mm long sample of 100% neutral parafinic oil. At the ^{17}O observe frequency (122 MHz) 150 kHz B_1 fields were achieved at 700 W using a sample of 5.5 mg of 40% labeled ^{17}O Gly in H_2O solution. While for ^{15}N detection (92 MHz) the power required to generate 100 kHz B_1 field was 675 W. Channel isolation was ~50 dB from ^{1}H to the broadband port, and at least 25 dB in the opposite direction depending on the observed nucleus. The spectra obtained using this transmission line probe are presented in Figs. 4 and 5 of this manuscript.

4. Summary

High performance NMR capabilities in solution, solids, and imaging have been demonstrated in the ultra wide bore 900 MHz NMR magnet. The NMR measurements clearly indicate that this newly available ultra wide bore magnet is of high quality in terms of field homogeneity and stability and is capable of performing a wide variety of scientific applications, ranging from materials research to macromolecular biological structure determination and non-invasive MR imaging. This 900 MHz Ultra Wide Bore NMR User Facility will be open for users in August 2005. Applications for the 900 MHz spectrometer time are currently being accepted. Interested scientists are encouraged to review sample spectra and other relevant information at http://nmr.magnet.fsu.edu/. The application forms and a description of the application process can be found at http://nmr.magnet.fsu.edu/facilities/900_105mm_TLH-ss.htm.

Note added in proof

The UWB 900 was successfully re-energized from 894 MHz to 900 MHz on September 8, 2005.

Acknowledgments

The ultra wide bore 900 MHz NMR at the NHMFL is supported by NSF and by the State of Florida. The

research on ^{17}O NMR spectroscopy and pulse sequence development activities are supported by NSF (MCB 0235774) to T.A.C. and R.F. The research on M2 Protein is supported by NSF (MCB 0235774) and NIAID (R01-23007-19) to T.A.C. and R.F. The research on mouse brain anatomy is supported by NIH (P41-RR16105) to S.C.G. Additionally, the authors would like to thank Dr. Helene Benveniste of Brookhaven National Laboratory for supplying fixed samples for preliminary imaging evaluations. This publication is dedicated to the memory of Jack E. Crow, Founding Director of the NHMFL an extraordinary scientific and technological visionary.

References

[1] W.D. Markiewicz, I.R. Dixon, C.A. Swenson, W.S. Marshall, T.A. Painter, S.T. Bole, T. Cosmus, M. Parizh, M. King, G. Ciancetta, 900 MHz wide bore NMR spectrometer magnet at NHMFL, IEEE Trans. Appl. Supercon. 10 (2000) 728–731.

[2] C.A. Swenson, Y.M. Eyssa, W.D. Markiewicz, Quench protection heater design for superconducting solenoids, IEEE Trans. Magn. 32 (1996) 2659–2662.

[3] I.R. Dixon, R.P. Walsh, W.D. Markiewicz, C.A. Swenson, Mechanical properties of epoxy impregnated superconducting solenoids, IEEE Trans. Appl. Supercon. 32 (1996) 2917–2920.

[4] C.A. Swenson, W.D. Markiewicz, Persistent joint development for high field NMR, IEEE Trans. Appl. Supercon. 9 (1999) 185–188.

[5] I.R. Dixon, W.D. Markiewicz, P. Murphy, T.A. Painter, Quench detection and protection of the wide bore 900 MHz NMR magnet at the NHMFL, IEEE Trans. Appl. Supercon. 14 (2004) 1260–1263.

[6] T.A. Painter, I.R. Dixon, W.D. Markiewicz, Voltage spike and magnet quench behavior in the NHMFL 900 MHz Bucket test, IEEE Trans. Appl. Supercon. 14 (2004) 1613–1616.

[7] W.D. Markiewicz, I.R. Dixon, Y.M. Eyssa, J. Schwartz, C.A. Swenson, S. Van Sciver, H.J. Schneider-Muntau, 25 T high resolution NMR magnet program and technology, IEEE Trans. Magn. 32 (1996) 2586–2589.

[8] T. Shimizu, K. Hashi, A. Goto, M. Tansyo, T. Kiyoshi, S. Matsumoto, H. Wada, T. Fujito, K. Hasegawa, N. Kirihara, Overview of the development of high-resolution 920 MHz NMR in NIMS, Phys. B Condens. Matter (2004) 346–347, 528–530..

[9] I.R. Dixon, W.D. Markiewicz, W.W. Brey, K.K. Shetty, Performance of the ultra wide bore 900 MHz NMR magnet at the National High Magnetic Field Laboratory, Applied Superconductivity Conference, (2004).

[10] G. Gabrielse, J. Tan, Self-shielding superconducting solenoid systems, J. Appl. Phys. 63 (1988) 5143–5148.

[11] Y. Iwasa, Microampere flux pumps for superconducting NMR magnets. Part I: basic concept and microtesla flux measurement, Cryogenics 41 (2001) 385–391.

[12] W.D. Markiewicz, Current injection for field decay compensation in NMR spectrometer magnets, IEEE Trans. Appl. Supercon. 12 (2002) 1886–1890.

[13] K. Pervushin, R. Riek, G. Wider, K. Wuthrich, Attenuated T_2 relaxation by mutual cancellation of dipole–dipole coupling and chemical shift anisotropy indicates an avenue to NMR structures of very large biological macromolecules in solution, Proc. Natl. Acad. Sci. USA 94 (1997) 12366–12371.

[14] J. Wang, S. Kim, F. Kovacs, T.A. Cross, Structure of the transmembrane region of the M2 protein H^+ Channel, Protein Sci. 10 (2001) 2241–2250.

[15] V. Lemaitre, M.E. Smith, A. Watts, A review of oxygen-17 solid-state NMR of organic materials—towards biological applications, Solid State Nucl. Magn. Reson. 26 (2004) 215–235.

[16] R.R. Ketchem, W. Hu, T.A. Cross, High-resolution conformation of gramicidin-A in a lipid bilayer by solid-state NMR, Science 261 (1993) 1457–1460.

[17] R.R. Ketchem, B. Roux, T.A. Cross, High-resolution polypeptide structure in a lamellar phase lipid environment from solid state NMR derived orientational constraints, Structure 5 (1997) 1655–1669.

[18] D.D. Busath, The use of physical methods in determining gramicidin channel structure and function, Annu. Rev. Physiol. 55 (1993) 473–501.

[19] F. Tian, T.A. Cross, Cation transport: an example of structural based selectivity, J. Mol. Biol. 285 (1999) 1993–2003.

[20] J.F. Hinton, W.L. Whaley, D. Shungu, R.E. Koeppe, F.S. Millett, Equilibrium binding constants for the group-I metal-cations with gramicidin-A determined by competition studies and Tl+-205 nuclear-magnetic-resonance spectroscopy, Biophys. J. 50 (1986) 539–544.

[21] J. Hu, E.Y. Chekmenev, Z. Gan, P.L. Gor'kov, S. Saha, W.W. Brey, T.A. Cross, Ion solvation by channel carbonyls characterized by ^{17}O solid state NMR at 21 T, J. Am. Chem. Soc. (2005) (in press).

[22] P.J. Carroll, P.L. Stewart, S.J. Opella, Structures of two model peptides: *N*-acetyl-D,L-valine and *N*-acetyl-L-valine-L-leucine, Acta Cryst. C 46 (1990) 243–246.

[23] M. Hohwy, N.C. Nielsen, Elimination of high order terms in multiple pulse nuclear magnetic resonance spectroscopy: application to homonuclear decoupling in solids, J. Chem. Phys. 106 (1997) 7571–7586.

[24] C.H. Wu, A. Ramamoorthy, S.J. Opella, High-resolution heteronuclear dipolar solid-state NMR spectroscopy, J. Magn. Reson. A 109 (1994) 270–272.

[25] A. Ramamoorthy, C.H. Wu, S.J. Opella, Three-dimensional solid-state NMR experiment that correlates the chemical shift and dipolar coupling frequencies of two heteronuclei, J. Magn. Reson. B 107 (1995) 88–90.

[26] R. Jelinek, A. Ramamoorthy, S.J. Opella, High-resolution three-dimensional solid-state NMR spectroscopy of a uniformly ^{15}N-labeled protein, J. Am. Chem. Soc. 117 (1995) 12348–12349.

[27] H. Benveniste, S.J. Blackband, MR microscopy and high resolution small animal MRI: applications in neuroscience research, Prog. Neurobiol. 67 (2002) 393–420.

[28] B. McDaniel, H. Sheng, D.S. Warner, L.W. Hedlund, H. Benveniste, Tracking brain volume changes in C57BL/6J and ApoE-deficient mice in a model of neurodegeneration: a 5-week longitudinal micro-MRI study, NeuroImage 14 (2001) 1244–1255.

[29] J.M.B. Wilson, M.S. Petrik, S.C. Grant, S.J. Blackband, J. Lai, C.S. Shaw, Quantitative measurement of neurodegeneration in an ALS-PDC model using MR microscopy, NeuroImage 33 (2004) 336–343.

[30] J. Schaefer, R.A. McKay, Multi-tuned single coil transmission line probe for nuclear magnetic resonance spectroscopy, US Patent: 5,861,748 (1999).

[31] C.M. Rienstra, Solid State Nuclear Magnetic Resonance Methodology for Biomolecular Structure Determination, in Chemistry, MIT (1999).

[32] A. Steinschneider, M.I. Burgar, A. Buku, D. Fiat, Labeling of amino-acids and peptides with isotopic oxygen as followed by O-17-NMR, Int. J. Pept. Protein Res. 18 (1981) 324–333.